Accepted Manuscript

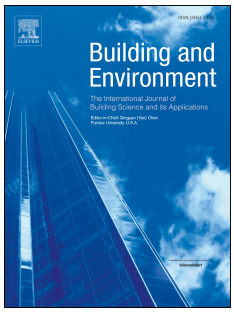

Characterizing dynamic transmission of contaminants on a surface touch network

Shenglan Xiao, Yuguo Li, Hao Lei, ChaoHsin Lin, Sharon L. Norris, Xinyan Yang, Pengcheng Zhao

PII: S0360-1323(17)30583-8

DOI: 10.1016/j.buildenv.2017.12.015

Reference: BAE 5213

To appear in: *Building and Environment*

Received Date: 17 August 2017

Revised Date: 13 December 2017

Accepted Date: 14 December 2017

Please cite this article as: Xiao S, Li Y, Lei H, Lin C, Norris SL, Yang X, Zhao P, Characterizing dynamic transmission of contaminants on a surface touch network, *Building and Environment* (2018), doi: 10.1016/j.buildenv.2017.12.015.

Characterizing dynamic transmission of contaminants on a surface touch network

Shenglan Xiao[a,*], Yuguo Li[a], Hao Lei[a], ChaoHsin Lin[b], Sharon L Norris[b], Xinyan Yang[a], Pengcheng Zhao[a]

[a] Department of Mechanical Engineering, The University of Hong Kong, Pokfulam Road, Hong Kong SAR, China
[b] Environmental Control Systems, Boeing Commercial Airplanes, Everett, WA, USA

* Corresponding author:
Shenglan Xiao. E-mail: u3002980@hku.hk; Tel.: +852 60992752

Abstract (212 words)

Our understanding of the fomite transmission route of diseases remains at an empirical level. There are no data on how surface contamination is propagated by human touching. We designed a novel and effective benchtop experiment to investigate the dynamic transmission of contaminants on multiple environmental surfaces due to touching. The benchtop experiment setting design was based on an inflight norovirus outbreak. Hundreds of representative environmental surfaces in the plane were scaled down, and fluorescent particles were used as surrogate indicators of virus-laden aerosols. The fluorescent particles were initially carried by six index "patients" and then transmitted to other surfaces through the touching behavior of one hundred and twenty-four "passengers." The distributions of fluorescent particles were photographed by cameras when exposed to UV light and the acquired photos were processed using fluorescence imaging techniques to quantify fluorescent particles on each surface. The temporal diffusion of contaminated surfaces was found to follow an *S*-shaped logistic curve. The aisle seats were found to be more contaminated, which was consistent with the reported higher attack rates in passengers seating along the aisle in the outbreak. This study confirmed the findings of the logistic growth from the multi-agent simulations, and provided a possible mechanism for the role played by environmental surfaces in the fomite route of diseases.

Keywords: Benchtop experiments; Fomite transmission route; Quantitative measurement; Fluorescence imaging techniques; Logistic growth.

1. Introduction

People in modern society live, study, and work in indoor environments [1] most of the time,

and inevitably touch numerous surfaces in their daily activities. The surfaces around us may not be microscopically clean, and many studies have detected viruses [2-4], bacteria [5, 6], and fungi [7, 8] on indoor surfaces. Some of these microorganisms are pathogenic and could survive for several days or even months [9, 10], which provides possibilities for the fomite transmission of related gastrointestinal, skin, and respiratory infections [11]. Although once thought to be negligible [12, 13], the role of the fomite route in disease transmission is supported by many studies [14], including observational epidemiologic studies [15, 16], intervention studies [17, 18], and outbreak reports [19, 20].

Our understanding of the fomite route remains at an empirical level [18, 21]. Although it appears straightforward, information on the propagation process of contaminations on multiple surfaces is very limited. In indoor environments, the multiple surfaces are not independent but are linked by hands through human touching behavior, thus constructing a surface touch network [22]. Once one or some surfaces are contaminated in this network, contaminants can be passed by hands to a large number of surfaces, as long as the source of contamination is strong enough. Due to the diversity of network structures, the diffusion of contaminants on the surface network presents different temporal and spatial characteristics.

There have not been any studies of the surface network except Lei et al. [22]. Several mathematical models have been used to study how contaminants diffuse across multiple surfaces, such as the discrete-time Markov chain model [23], the differential equation model [24], and the multi-agent model [25], but few experiments have been conducted because the sequential detection of surface contaminations is a challenging task. Common techniques used to quantify microorganisms on multiple surfaces such as hybridization-based [26] and polymerase-chain-reaction-based techniques [27] have their limitations. Small samples wiped from an environmental surface do not reflect the overall degree of contaminations [28], while large samples or the original surfaces only allow one-time measurements. In this study, fluorescent particles were used as surrogate indicators. These emit visible light when exposed to UV light, and the luminance of emitted light monotonically increases with the quantities of particles [29], which enables multiple quantification measurements. Fluorescent particles have been used in several studies to measure the transfer of contaminants [30, 31] but usually on a small scale, such as on human hands, which cannot provide enough information about how contaminants are

transferred on a surface touch network.

Here, we describe a novel and effective benchtop experiment. Chips of different materials present in an environment of interest are placed on a large table in a temperature- and humidity-controlled room. Participants are instructed to touch the chips in a specific sequence, defined based on the observation data in the environment of interest. To demonstrate our new method, an inflight norovirus outbreak [20] was chosen as the scenario for the experiment, as shown in Fig. 1. Six passengers from the same tour group were considered as possible index patients. Since the first-class rows were screened off from the others, we only considered the transmission between passengers in economy class. During the 2.5-hour flight, 6 of 71 non-tour group passengers in economy class who were interviewed after the flight [20] developed the same kind of gastric illness. Statistics showed that sitting in an aisle seat was associated with the development of illness (P = 0.022, 1-sided Chi-square test). The modeling results in Lei et al. [22] also showed that the contamination conditions on surfaces of aisle seats were worse than others, and correspondingly passengers sitting there had higher infection risks.

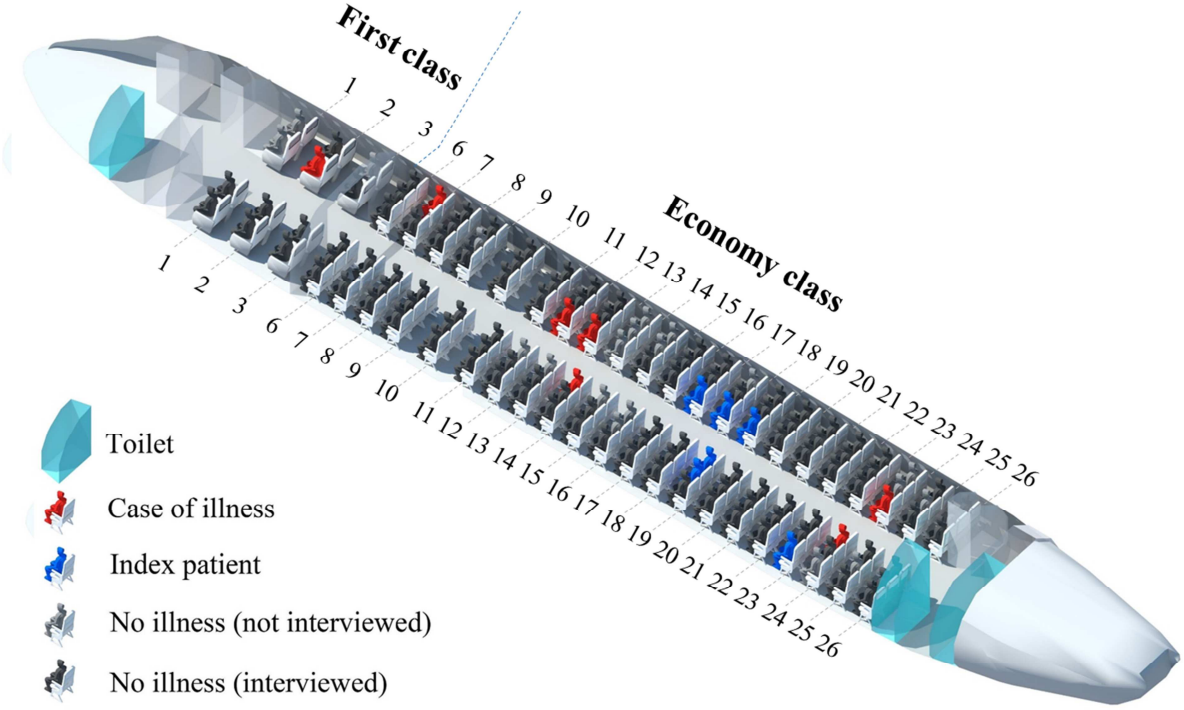

Fig. 1. The seating plan on the plane with the norovirus outbreak in October 2008, adapted from

Kirking et al. [20]. The index patients, infected passengers, and uninfected passengers (including both those interviewed and not interviewed) are marked with different colored symbols. Row numbers are marked, with Rows 1-3 representing first class and Rows 6-26 representing economy class.

In the benchtop experiment setting, hundreds of representative environmental surfaces in the economy class of the plane were scaled down and fluorescent particles on each surface were quantified using fluorescence imaging techniques. The quantification results were compared with the multi-agent modeling results in Lei et al. [22] and the attack rate distribution in Kirking et al. [20]. The results reported present the dynamic and rapid transmission of contaminants on multiple environmental surfaces, and confirm the findings from multi-agent simulations.

2. Methods

2.1 Materials

With low pigment residues and significant intensity changes to exposures [31], fluorescent particles from GloGerm^{TM} were selected in the experiments. The diameter of the chosen fluorescent particles is of the order of magnitude of 100 nm to 10 μm (Fig. S1), similar to that of human-exhaled droplets [24, 32]. The peak excitation wavelength of the fluorescent particles is about 375 nm (Fig. S2) in the range of UV light, so the particles are invisible without the UV light and thus do not interfere with the experiments. The peak emitted light is about 433 nm and can be recorded by cameras as it is in the range of visible light.

Fingerstalls were used to represent the hands of 124 passengers in the economy class of the plane [20]. The environmental surfaces considered in the study were porous (126 seatbacks, made of Dacron) and non-porous (126 tray tables, 168 armrests, and 2 toilets made of modified propylene polymer). Due to space limitations, all these surfaces were shrunken from that in the real plane at a specific proportion (5.17:1), which is about the ratio of hand length to fingertip length.

2.2 Measurements of transfer efficiencies

The transfer efficiencies of the fluorescent particles were measured as the input parameters for the simulations to avoid errors caused by the different transfer properties of fluorescent particles and virus-laden aerosols. As the transmission process could be highly influenced by finger touching force [33], the transfer efficiencies were investigated with different touching

forces.

As the first step, the range of touching forces was determined. An ordinary balance (SF-400, SIQI, Jinan, China, capacity: 7000 g, readability: 1g) was touched by fingers 1,000 times and the reading for each was recorded. The balance can reflect the pressure, enabling the touching force to be estimated.

The transfer efficiencies were measured using a homemade touching machine, as shown in Fig. 2. The device can specify the touching force as required and control the contacting duration. Three kinds of surface materials are typically used in the benchtop experiments. As such, four kinds of transfer efficiencies, i.e., from plastic pieces (modified propylene polymer) to fingerstalls, from fingerstalls to plastic pieces, from Dacron pieces to fingerstalls, and from fingerstalls to Dacron pieces, were respectively measured.

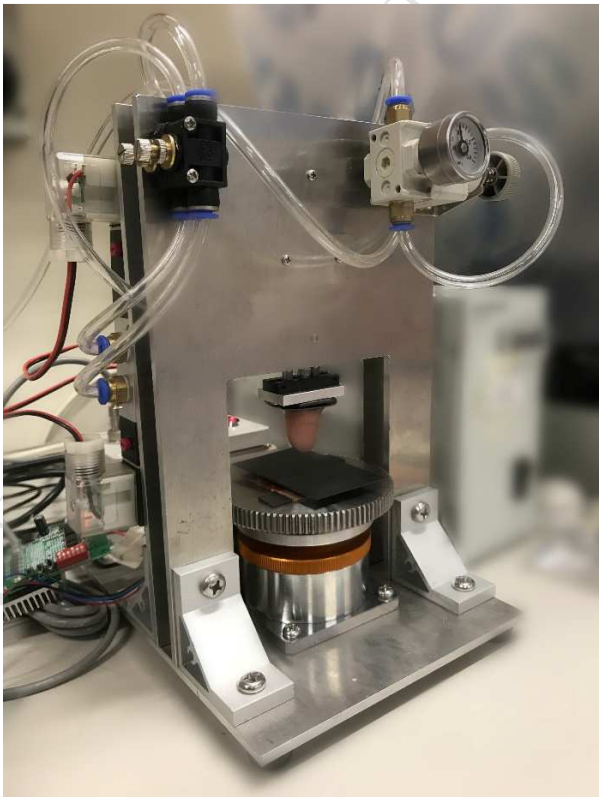

Fig. 2. The in-house developed touching machine that can specify both the touching force and contact duration as required.

The measurements of transfer efficiencies from plastic pieces to fingerstalls can be used as

an example of the process. First, weigh a clean piece with the analytical balance (Secura125-1S, Sartorius, Goettingen, Germany, capacity: 120 g, readability: 0.01 mg) and record the reading denoted as m_1. Second, apply fluorescent particles onto the piece uniformly with a spray and then weigh the piece with the analytical balance again, with the reading denoted as m_2. Third, fix a clean fingerstall onto the touching machine and touch the contaminated piece with a given force denoted as f. Fourth, weigh the touched piece on the analytical balance, and record the reading denoted as m_3. After collecting the data, the transfer efficiency TE was calculated as $\frac{m_3-m_1}{m_2-m_1}$ [33, 34] when the touching force was f. Other than the touching force, factors influencing the transfer process such as relative humidity, contacting time and moisture [33] were kept the same during the measurements. The other three types of transfer efficiencies were measured in a similar way.

2.3 Benchtop experiment setting

The benchtop experiment setting and its components are shown in Fig. 3A. The sketch of the economy class of the plane (Fig. 3B) was printed on a piece of waterproof paper (3000 by 900 mm) on the experiment table, and the height of the experiment chamber was designed to be 1000 mm to guarantee that the four photos taken by the four cameras could cover all the environmental surfaces. The environmental surface materials, namely Dacron and plastic pieces, were applied onto acrylic blocks of different heights on the waterproof paper, so when the participants touched one surface the others would not be accidentally contaminated. Pairs of soft magnetic sheets were used to connect the surface materials and the acrylic blocks, which kept the surface materials still when the participants touched the surfaces and allowed them to be taken away from the table during the calibration work.

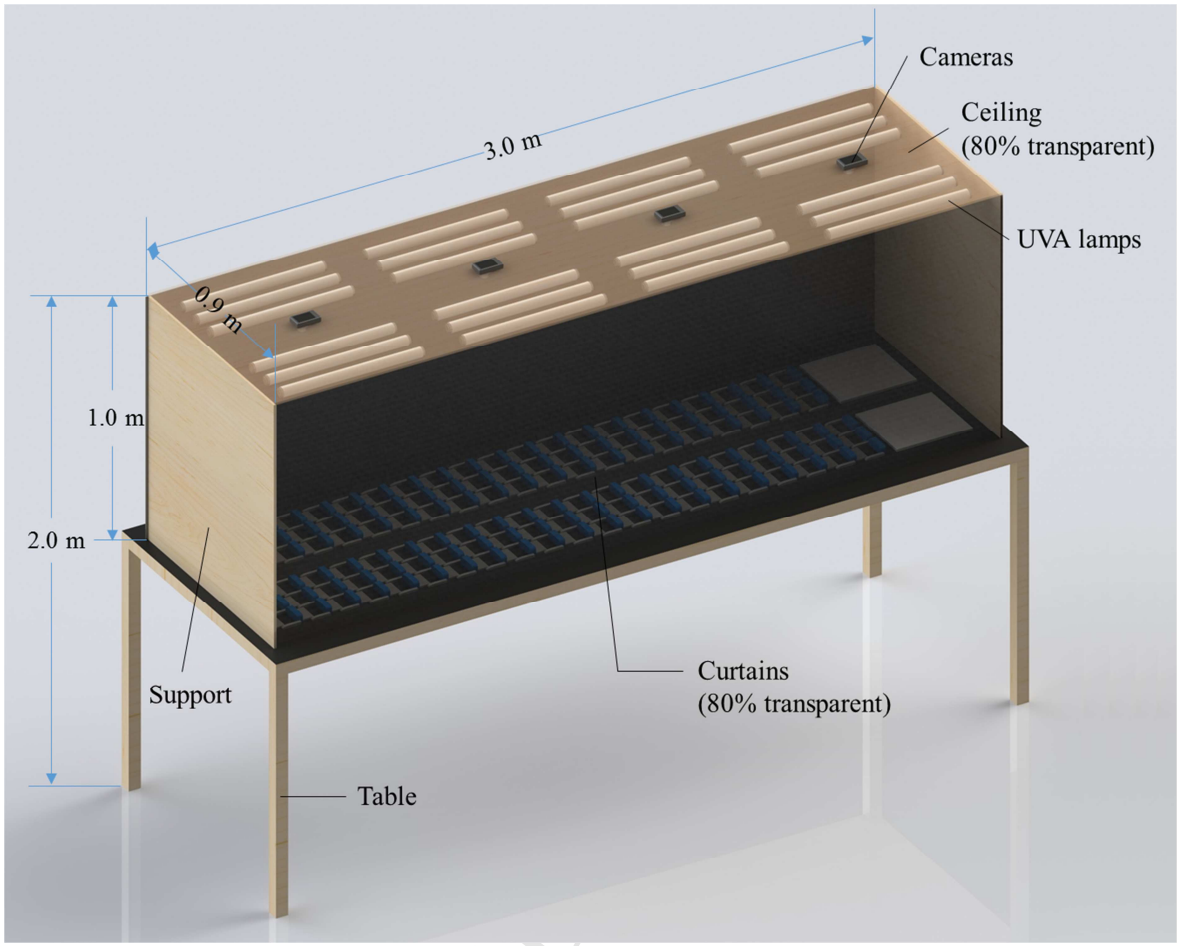

(A)

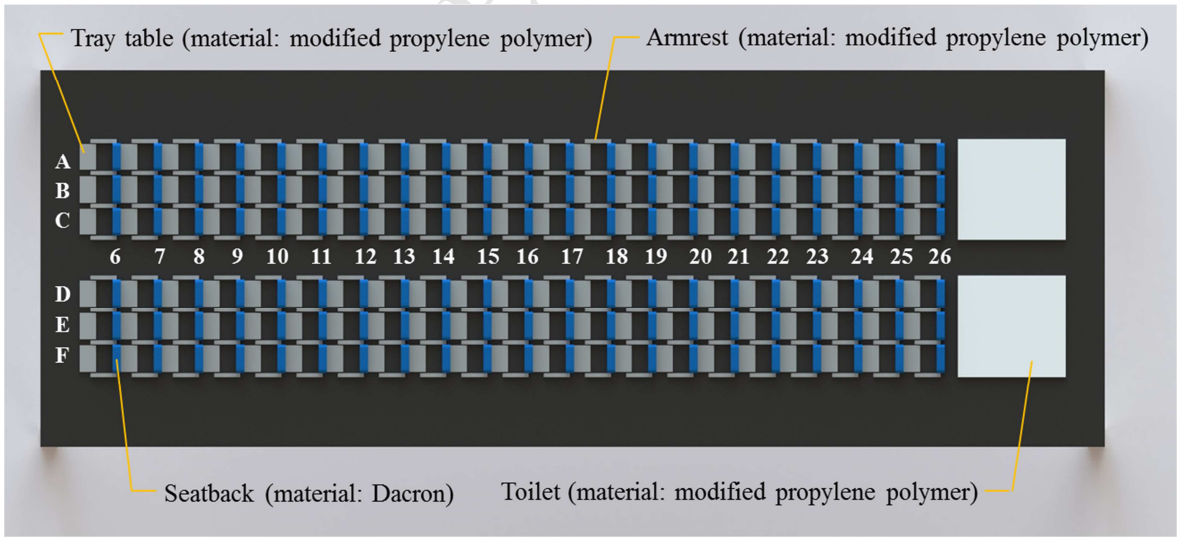

(B)

Fig. 3. (A) The physical layout of the benchtop experiment setting and its components. The ceilings and curtains were processed to be 80% transparent to show the internal settings. (B) The

plan of the airplane adapted from Kirking et al. [20]. The four kinds of surfaces were in fact black in color to contrast the emitted light of fluorescent particles, but different colors are used here to differentiate them.

In addition to the experiment table, several apparatuses were combined into the experiment chamber, as shown in Fig. 3A. Twenty-four Philips TL'K 40W (R) UV lamps were fixed on the inner side of the ceiling to make the UV light over the experiment table as homogeneous as possible. For safety, the UV lamps also emitted blue light to indicate whether they were open or closed. Four cameras (Sony DSC-WX350, 8-bit) took pictures through four holes on the ceiling. The cameras were responsible for four areas on the table and were controlled remotely via Wi-Fi to avoid shake when taking photos. The experiment chamber was surrounded by wood supports and black curtains. The curtains had reflective coating on the inside surface to reflect UV light onto the experiment table and prevent any injury to the participants.

2.4 Calibration

The experiment required calibration, as the distance between the surfaces and UV lamps or cameras could affect the luminance of fluorescent particles in the photos, and the thickness of fluorescent particles on the surfaces also influenced the intensities of the emitted light [29]. Moreover, since almost all digital cameras perform gamma correction (tone curve correction) to adjust pictures, the pixel values are not proportional to the number of photons that struck the image sensor during the exposure [35]. Therefore, the calibration was necessary to acquire the complex relationships between the intensities of emitted light and the amount of fluorescent particles for different surface positions.

In this study, the weighting factor W, defined as the mass of fluorescent particles per pixel in the photo, was used to represent the amount, and the net pixel signal strength k, defined as the pixel value (grey level) on a surface in the photo after the removal of the background, was used to represent the light intensity. The calibration process is as follows. First, prepare a clean surface and take the background photos with the UV lamps on. Second, apply fluorescent particles onto the clean surface uniformly with a spray and measure the total mass of particles on the surface with the analytical balance and then take result photographs with the UV lamps on. Finally, acquire the total pixel number and pixel values of the surface in both the background and result photos with the software MATLAB R2014a. The weighting factor W was calculated as the mass

of fluorescent particles divided by the total pixel number of the surface, while the net pixel signal strength *k* was calculated as the pixel value in the result photo minus that of the background photo.

2.5 Experiment procedures

According to the initial report of this outbreak [20] and the modelling study [22], we assumed that all the environmental surfaces were clean prior to the flight and did not consider the role of cabin staff on the contamination transmission. Since the cabin air was clean at cruising altitude [36], we ignored the deposition of virus-containing airborne droplets on most surfaces except for those around the index patients, and only considered the contamination caused by human surface touching behaviors. The surface touching sequences were kept the same for the experiments and simulations so the results could be compared. The touching sequences were generated based on assumptions in Table S1. Although the passengers shared the same rules of behavior, they did not act synchronously and did not touch the same surfaces for a specific behavior. Therefore, the generated sequences varied with each other. Five touching sequences were chosen for five sets of experiments and each set was repeated three times. In each experiment, 50 normal passengers were randomly selected to use the toilets during the flight, together with 6 index patients. They were assumed to spend the same time lengths using the toilets, so the flight cruise period (150 minutes) could be divided equally into 56 rounds. In each round, following the sequence, one passenger represented by the corresponding fingerstall went to the toilets and touched aisle seatbacks on the way and back due to the plane's instability. In addition, some of the seated passengers, represented by the corresponding fingerstalls, were assumed to touch some surrounding surfaces. After each round, the UV lamps were turned on and photos were taken with the four cameras.

With the relationships acquired in the calibration, the photos could be processed. The signal strength of every pixel on the surfaces in the photos was acquired with MATLAB R2014a. According to the acquired relationship, the mass of fluorescent particles per pixel was calculated. Finally, the total mass of particles on a surface was acquired according to Equation 2 from Ivancic et al. [29].

3. Results and discussion

3.1 Transfer efficiencies of fluorescent particles between surfaces

220 Fig. S3 shows the frequency distribution of the finger touching forces. The ordinary balance
221 (7000 g×1g) used to measure the touching force had the maximum relative error of 0.15%.
222 According to the one-sample Kolmogorov-Smirnov test [36] (P = 0.09), at a 5% level of
223 significance, finger touching forces could be assumed to follow a normal distribution, N(11.80,
224 1.97^2), consistent with the measurement results from Zhang [38]. Fig. S3 shows that the finger
225 touching forces ranged from 6 to 17 N, so the transfer efficiencies were measured within this
226 range.

227 Fig. 4 shows the measured transfer efficiencies of fluorescent particles between surfaces
228 with different touching forces. The analytical balance (120 g×0.01 mg) to measure the weight of
229 fluorescent particles on fingerstalls and plastic pieces had the maximum relative error of 0.07%.
230 The direction of transfer was found to have an effect on the transfer efficiencies. For example,
231 the transfer efficiency from fingerstalls to Dacron pieces was always higher than for the reverse.
232 Similar findings were reported in measurements for bacteria [39] and viruses [40]. The type of
233 surface material was found to greatly influence transfer efficiencies. For example, higher values
234 were found in the transfer efficiency from nonporous materials (plastic pieces) to fingerstalls
235 than from porous materials (Dacron pieces) to fingerstalls. Several studies have observed similar
236 phenomena for microorganisms with nonporous materials (such as faucet handles and phone
237 receivers) and porous materials (such as dishcloths and sponges) [34, 41].
238

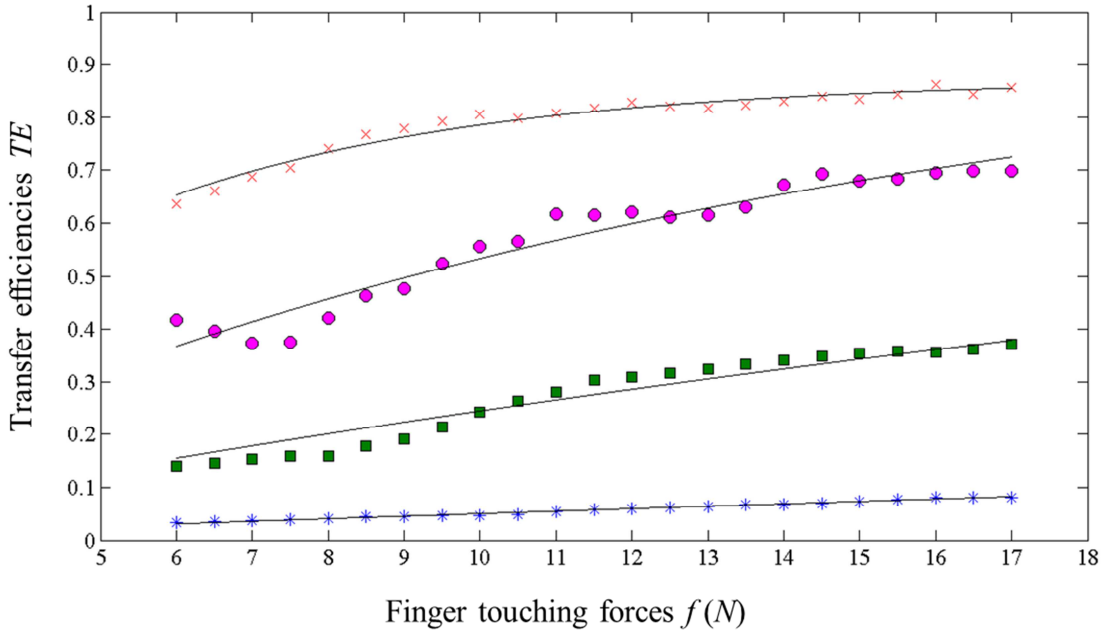

Fig. 4. The relationships between finger touching forces and measured transfer efficiencies from fingerstalls to Dacron pieces, from Dacron pieces to fingerstalls, from fingerstalls to plastic pieces, and from plastic pieces to fingerstalls. Different kinds of transfer efficiencies are marked with different symbols in different colors. The fitted curves are in black, and their fitting function was $TE = c_1(1 - c_2^f)$ (c_1 and c_2 denote the underdetermined coefficients) as shown in Table 1.

In general, the measured transfer efficiencies increased with the touching forces, consistent with similar studies of microorganisms such as hepatitis A virus (HAV) [42]. No model was available to describe the roles of touching forces, so the measured data were fitted with a common function $TE = c_1(1 - c_2^f)$ (c_1 and c_2 denote the underdetermined coefficients, and c_1 was no more than 1) via least squares regression, as shown in Table 1. The function satisfies features of the relationship, in that the transfer efficiency is 0 when the touching force equals 0, and it is always in the range of 0-1. The standard errors of the regression S were all less than 0.03 and the coefficients of determination R^2 were all larger than 90%, indicating good agreement between the fitting curves and sample data [43, 44].

256 **Table 1** The functions for the fitted curves in Figs. 4, 5, and 6.

Figures	Descriptions	Functions	S [a]	R^2 [b]
Fig. 4	The relationship between finger touching forces *f (N)* and measured transfer efficiencies *TE* from fingerstalls to Dacron pieces	$TE = 0.5405 \times (1 - 0.9903^f)$	0.0018	0.9878
	The relationship between finger touching forces *f (N)* and measured transfer efficiencies *TE* from Dacron pieces to fingerstalls	$TE = 0.8729 \times (1 - 0.7948^f)$	0.0122	0.9644
	The relationship between finger touching forces *f (N)* and measured transfer efficiencies *TE* from fingerstalls to plastic pieces	$TE = 1 - 0.9724^f$	0.0218	0.9350
	The relationship between finger touching forces *f (N)* and measured transfer efficiencies *TE* from plastic pieces to fingerstalls	$TE = 0.9922 \times (1 - 0.9258^f)$	0.0281	0.9425
Fig. 5	The relationship between pixel signal strength *k* and mass of fluorescence particles per pixel *W* (μg/pixel) for Seat 6A	$W = \sqrt{\frac{22.6332}{122.0664 - k} - 0.1854}$	0.1076	0.9623
	The relationship between pixel signal strength *k* and mass of fluorescence particles per pixel *W* (μg/pixel) for Seat 7A	$W = \sqrt{\frac{16.2856}{126.0449 - k} - 0.1292}$	0.1031	0.9654
	The relationship between pixel signal strength *k* and mass of fluorescence particles per pixel *W* (μg/pixel) for Seat 8A	$W = \sqrt{\frac{12.4171}{128.9467 - k} - 0.0963}$	0.1096	0.9609

	The relationship between pixel signal strength k and mass of fluorescence particles per pixel W (μg/pixel) for Seat 9A	$W = \sqrt{\frac{17.0907}{126.8107 - k} - 0.1348}$	0.0948	0.9708
	The relationship between pixel signal strength k and mass of fluorescence particles per pixel W (μg/pixel) for Seat 10A	$W = \sqrt{\frac{22.9143}{123.5858 - k} - 0.1854}$	0.1062	0.9633
Fig. 6	The relationship between time t (Round) and the number of contaminated aisle seatback surfaces N	$N = 42 \times 0.4767(\frac{3.0978}{1 + e^{-0.0857t+0.7408}} - 1)$	1.0038	0.9944
	The relationship between time t (Round) and the number of contaminated surfaces N	$N = 422 \times 0.1811(\frac{6.5218}{1 + e^{-0.0319t+1.7088}} - 1)$	3.0984	0.9971

a S refers to the standard errors of the regression;

b R^2 refers to the coefficients of determination.

3.2 Relationships between the emitted light intensities and fluorescent particle amounts

Fig. 5 shows the calibration curves used to convert the net pixel signal strength k to weighting factor W of fluorescent particles for the surfaces of Seats 6A, 7A, 8A, 9A, and 10A. For the same position, the maximum net pixel signal strength was about 130, much less than almost 250 found by Ivanic et al. [29]. This was induced by blue light emitted from the UV lamps. As shown in original photos such as Fig. S4a, uncontaminated surfaces were also visible, indicating that the pixel values in the background photo were not low. Thus, after the removal of the background, as shown in Fig. S4b, the net pixel signal strength was not very high.

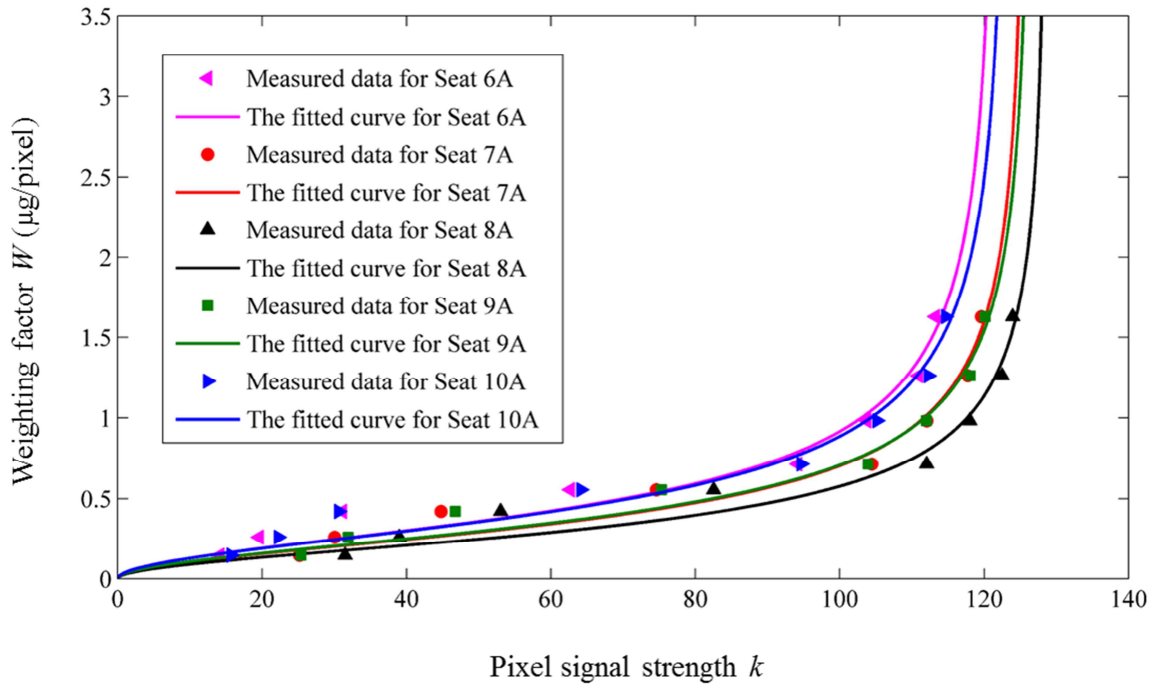

Fig. 5. Calibration curves to convert net pixel signal strength to the mass of fluorescent particles per pixel of surfaces for Seats 6A, 7A, 8A, 9A, and 10A, shown in Fig. 3B and S4. Measured data for different positions are marked with different symbols in different colors. The fitted curves share the same colors with the corresponding data, and their fitting function is $W = \sqrt{\frac{c_3}{c_4 - k} - \frac{c_3}{c_4}}$ (c_3 and c_4 denote the underdetermined coefficients) as shown in Table 1.

The relationship between the net pixel signal strength k and the weighting factor W was influenced by the layering effects of fluorescent particles and camera nonlinearity. On one hand,

more than one layer of fluorescent particles is usually present on a surface, and less photons which struck the image sensors during the exposure were emitted from the lower layers due to the less available excitation energy and increased scattering of emitted light. Thus, the number of photons increased with the quantities of fluorescent particles at a gradually decreasing growth rate [29]. On the other hand, due to the gamma correction performed by digital cameras, the pixel values also increased with the number of photons [35] at a gradually decreasing growth rate. As a joint result of layering effects and camera nonlinearity, the net pixel signal strength *k* increased monotonically with the weighting factor *W*, but the growth rate gradually slowed down, which was consistent with the findings of Ivancic et al. [29].

To describe the relationship between the net pixel signal strength *k* and the weighting factor *W*, Ivancic et al. [29] used a six-order polynomial function to fit the measured data and achieved a high coefficient of determination R^2 of 99.94%, but this function is not monotonic with the net pixel signal strength *k* ranging from a minimum of 0 to the maximum of 255. Therefore, the function $W = \sqrt{\frac{c_3}{c_4 - k} - \frac{c_3}{c_4}}$ (c_3 and c_4 denote the underdetermined coefficients) was used in this study to fit data via least squares regression, as shown in Table 1. This function satisfies the features of the relationship, in that when the weighting factor *W* increases, the net pixel signal strength *k* grows at a gradually slower rate. The standard errors of the regression *S* were all less than 0.11 and the coefficients of determination R^2 were all larger than 95%, indicating good agreements between the fitting curves and sample data [43, 44].

For different positions, such as Seats 6A, 7A, 8A, 9A, and 10A in Figs. 3B and S5, the acquired relationships differ slightly. As the Seat 8A position was closest to the UV lamps and cameras (Fig. S5), the fluorescent particles received the most excitation energy from the UV lamps and more of the emitted light could reach the camera, so the same amount of fluorescent particles showed the most brightness on it. Similarly, as the positions of Seats 7A and 9A and those of Seats 6A and 10A were symmetrical (Fig. S5), the same amount of fluorescent particles showed similar brightness on each pair, respectively.

3.3 Logistic growth of the number of contaminated surfaces

Fig. S6 shows the processed photos showing fluorescent particles on surfaces with the background removed in one experiment at different time points. Fig. 6 shows the growth of the

number of contaminated surfaces. The large scatter between individual experiment results was caused by the randomness of human behaviors rather than measuring errors. Passengers randomly touch the surrounding surfaces and randomly go to the toilets, which are inevitable and unpredictable, so experiment results varied with each other. Thereby, the strategy to control the diffusion of surface contaminations should be developed based on average results rather than an individual one.

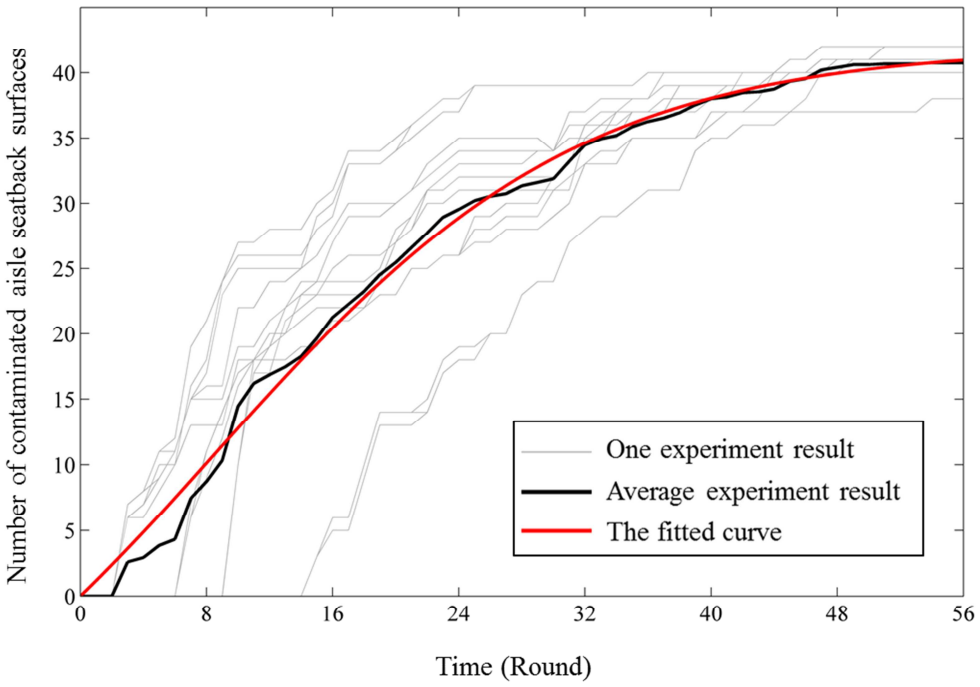

(a)

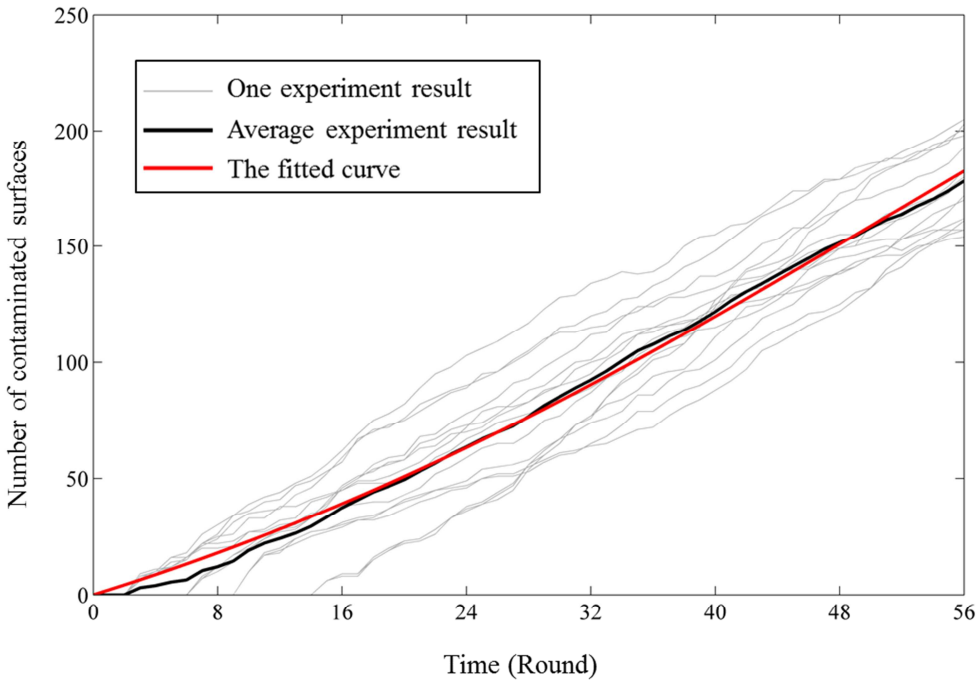

(b)

Fig. 6. Growth of the number of contaminated surfaces: (a) 42 aisle seatback surfaces; (b) the total 422 surfaces. Each graph shows 15 experiment results (gray lines), the average of 15 experiment results (the black line), and the fitted logistic curve (the red line). The fitting function is $N = N_{max}e^{-c_6}(\frac{1+e^{c_6}}{1+e^{-c_5\,t+c_6}} - 1)$ (N_{max} = 42 for Fig. 6a and N_{max} = 422 for Fig. 6b, respectively; c_5 and c_6 denote the underdetermined coefficients) as shown in Table 1.

As shown in Figs. S6 and 6a, for aisle seatback surfaces, the diffusion of contaminated surfaces followed an *S*-shaped logistic curve in time, consistent with the multi-agent simulation results [22]. In the first stage, the number of contaminated aisle seatback surfaces was small and thus the possibility for clean fingerstalls to be contaminated by dirty surfaces was small. Most transmissions then occurred between clean fingerstalls and clean surfaces. A growth of contaminated surfaces increased the conversion from clean fingerstalls to dirty fingerstalls, which in turn accelerated the growth of contaminated surfaces. Therefore, in the first stage, the growth of the number of contaminated aisle seatback surfaces became rapid. In the latter stage, the number became high and thus clean fingerstalls could easily be contaminated. Most transmissions at this point occurred between dirty fingerstalls and dirty surfaces. The increase of contaminated surfaces decreased the possibility of transmissions from dirty fingerstalls to clean surfaces, which in turn slowed down the spread of contaminated surfaces. Therefore, in the latter

stage, the growth of the number of contaminated aisle seatback surfaces slowed down until reaching saturation.

Analogously, the diffusion of the total contaminated surfaces should have also followed an *S*-shaped curve in time, but as the flight cruise periods (56 rounds, 150 minutes) were too short for contamination of the total surfaces, the number of contaminated surfaces was relatively small throughout compared with the total surface number (422). Therefore, the diffusion was limited to the first stage of the *S*-shaped curve and the growth rate kept accelerating until the end, as shown in Fig. 6b. At the end of the cruise period (Round 56), the number of contaminated surfaces was about 178, which was small compared with the prediction from simulation results of about 300 [22]. There are two possible reasons to account for the difference between the simulations and experiments. First, in the simulations it was assumed that the fluorescent particles were uniformly distributed on the entire areas of the surfaces, so a clean fingerstall touching a dirty surface always resulted in the transmission of contamination. However, in the experiments, only some regions of a surface could be contaminated while others might not have been, so when a clean fingerstall touched the clean region of contaminated surfaces, no transmission occurred. Second, in the simulations a surface was counted as contaminated even with only a tiny amount of contaminant on it, while in the experiments the light emitted from a tiny amount of fluorescent particles was undetectable, so the amount could not be measured until it accumulated to the minimum dose.

3.4 Severe contamination conditions on aisle surfaces

The pixel values in the photos in Fig. S6 were converted into the amounts of fluorescent particles on surfaces according to the calibration curves in Fig. 5. Degrees of surface contamination were divided into three classes, scanty ($\leqslant$1 μg/cm^2), moderate (>1-20 μg/cm^2), and heavy contaminations (>20 μg/cm^2). Fig. 7 shows the average percentages of aisle and non-aisle surfaces from 15 experiments, with scanty, moderate, and heavy contaminations at different time points. Aisle surfaces refer to surfaces in aisle seats, including 42 seatback surfaces, 42 tray table surfaces, and 42 armrest surfaces of seats in Rows C and D. Non-aisle surfaces refer to surfaces in non-aisle seats, including 84 seatback surfaces, 84 tray table surfaces, and 84 armrest surfaces of seats in Rows A, B, E, and F. Note that here the 42 armrests between Rows B and C and between Rows D and E are not counted as aisle or non-aisle surfaces.

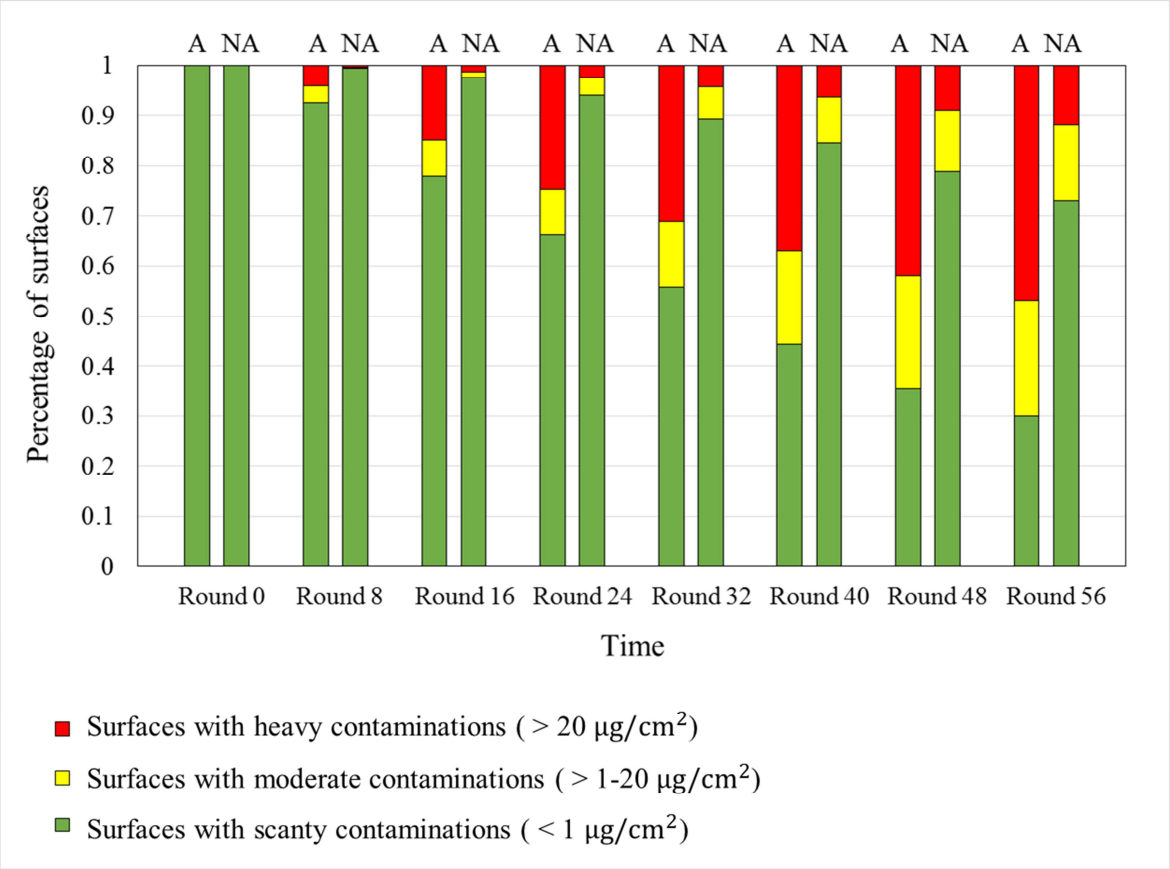

Fig. 7. Percentage of aisle (A) and non-aisle (NA) surfaces with scanty, moderate, and heavy contaminations at different time points. The result was the average of 15 experiments. Different levels of contamination are marked in different colors.

As shown in Fig. 7, the fluorescent particles kept spreading to clean surfaces on both the aisle and non-aisle surfaces over time, so the percentage of surfaces with scanty contaminations decreased while the other two percentages increased, respectively. However, the aisle surfaces became moderately or heavily contaminated faster than the non-aisle surfaces. At the end of the cruise period (Round 56), greater proportions of aisle surfaces were found with moderate (P=0.050, Chi-square test) and heavy contaminations (P=0.000, Chi-square test), respectively, indicating more severe contamination conditions on the aisle surfaces. Passengers seated on the aisle seats were more likely to get sick, as they were surrounded by more severe contaminated surfaces [45]. This was consistent with the higher infection risks predicted by simulations [22] and the higher attack rates found in this outbreak [20] for the passengers seated in the aisle seats.

Aisle seatbacks play an important role in the transmission of contaminations in the air cabins, which probably led to the more severe contamination condition on aisle surfaces. Normal passengers and index patients were all very likely to touch aisle seatbacks on their way to the toilet and back. Therefore, aisle seatbacks were touched at a higher frequency than other seatbacks and became the medium transmitting contaminants from index patients to normal passengers. According to Fig. 4, the transfer efficiency from fingerstalls to porous materials is much higher than that from porous materials to fingerstalls, so a large amount of contaminants remained on the aisle seatbacks rather than spreading to other surfaces. Seated passengers were likely to touch the surfaces around them, so the hands of passengers sitting on the aisle seats were likely to more contaminated, and thus brought more contaminants to the aisle armrests and tray tables. Thus, aisle surfaces, including seatbacks, armrests, and tray tables, were more likely to be severely contaminated than non-aisle surfaces. Similar phenomena were also found in hospitals, where the surfaces around patients that were touched frequently by healthcare workers and patients were more likely to be contaminated with pathogens than other sites [13, 46, 47]. The environmental infection control measures in air cabins and hospitals should be informed by these observations, and more attention should be paid to frequently touched surfaces, which is consistent with the recommendations from Centers for Disease Control and Prevention [48].

3.5 Comparison of the benchtop experiment results with multi-agent simulation results

Figs. 8a and 8b show distributions of fluorescent particles on 422 surfaces from 15 experiments and 15 simulations using a multi-agent model [22], respectively. Comparing the two distributions with that of the actual cases of illness in the outbreak, it was noticeable that the environmental surfaces around the infected passenger seating in Seat 7A were clean. It's because the actual touching sequences in the outbreak were unknown and might differ from the assumed the assumed five touching sequences in the experiments and simulations. Due to the randomness of human behaviors, the distribution of infections in the outbreak was merely one of numerous possible situations, so the position of an individual infected passenger did not have the statistical significance. In contrast, the characteristic of the overall distribution in the outbreak, that sitting in an aisle seat was associated with the development of illness, was statistically significant (P = 0.022, Chi-square test), which is consistent with the experiment and simulation results shown in Figs. 8a and 8b.

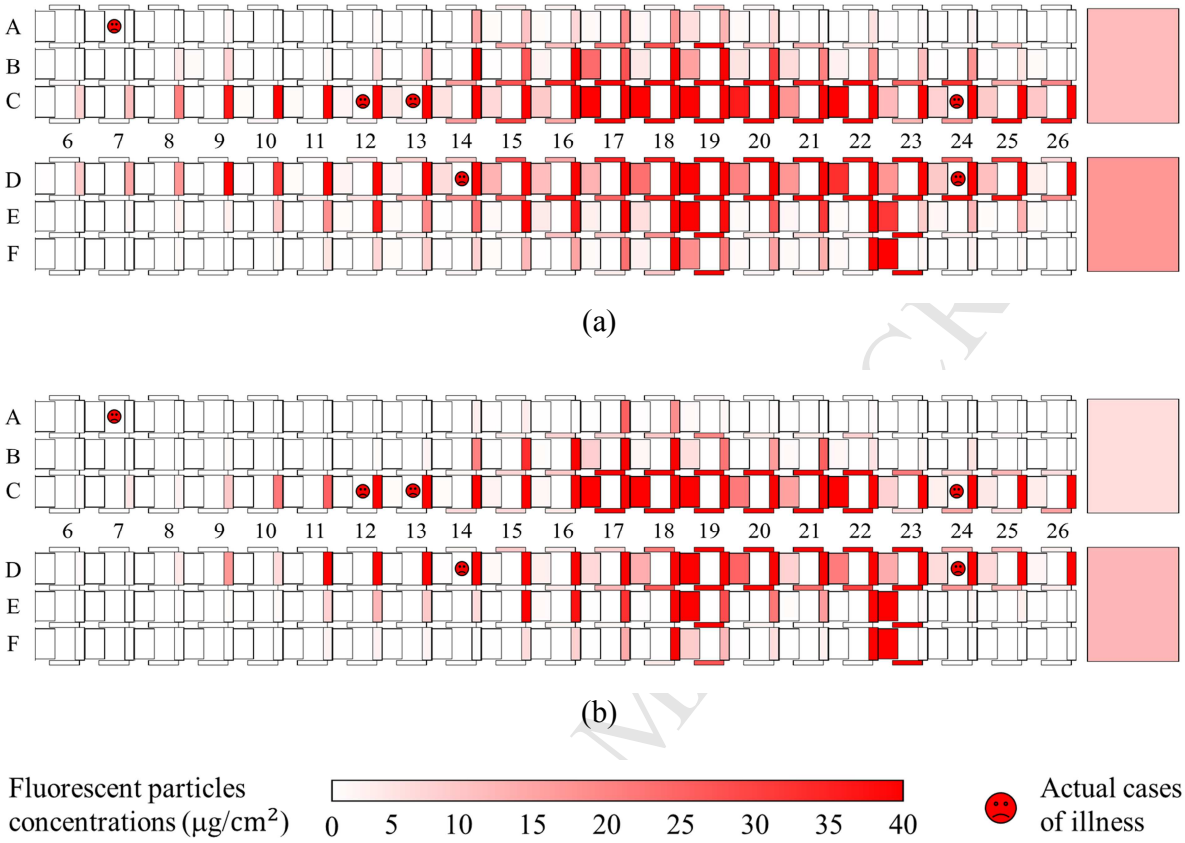

Fig. 8. Distributions of fluorescent particles on 422 environmental surfaces. (a) Average of 15 experiments results. (b) Average of 15 multi-agent simulations. The actual cases of illness in the outbreak were marked with red symbols. Different levels of concentrations on surfaces of fluorescent particles are represented by the intensity of the red shading. The concentrations over 40 μg/cm^2 are the same color as those of 40 μg/cm^2.

The two distributions shown in Figs. 8a and 8b were broadly similar, but the contaminations on many surfaces in the simulation results were less severe than those in the experiment results. Assuming that the fluorescent particles were uniformly distributed over the entire surface areas led to underestimation in the simulation results. Therefore, in the simulations, when a clean fingerstall touched a contaminated surface, the concentration on the contact area of the surface was the average concentration on the entire surface, which was usually low, so the transmission from contaminated surfaces to clean fingerstalls was limited.

As mentioned, the distribution on most surfaces was not uniform in reality. Passengers were

more likely to touch a specific region of the surfaces in some situations. For examples, when touching the aisle seatbacks on their way to the toilet and back, they tended to touch regions close to the aisle, and when seated passengers put their hands on the armrests they rarely touched the regions that adjoined the backs of the seats. Thus, when a clean fingerstall touched a contaminated surface, the contact areas were generally the frequently touched regions, where the concentration of contaminants was much higher than the average concentration. Therefore, in the experiments, the transmission from contaminated surfaces to clean fingerstalls was enhanced in the experiments, which improved the overall effectiveness of transmission from the source to other surfaces.

3.6 Limitations

Our benchtop experiments have four limitations. First, errors may be introduced by the measuring instruments. For example, the bit level of cameras can influence the precision of the calibration curves. Cameras with higher bit levels had more grey levels, and could significantly reduce the relative error during measurements of the pixel signal strength k in Fig. 5. The 8-bit cameras used in the experiments had merely 256 grey levels, with the maximum relative error to measure the pixel signal strength of about 7.00%. In contrast, the 10-bit cameras have 1024 grey levels with the maximum relative error of about 1.75%, and 12-bit cameras have 4096 grey levels with the maximum relative error of about 0.87%. In future studies, more accurate instruments could be used in the measurements.

Second, quantification cannot be conducted when there is a large amount of fluorescent particles on surfaces. As shown in the calibration curve (Fig. 5), when the fluorescent particles accumulated to a certain amount, the intensity of the emitted light hardly changes, due to the layering effects [29]. However, this does not matter if a proper scale of the amount of fluorescent particles is chosen in the experiments. According to the exponential dose-response relationship described by the Wells-Riley model [49], when surfaces are already very severely contaminated, the infection risk caused by touching them is very high and does not change to any great extent. Therefore, it is far more important to distinguish severely contaminated surfaces from others than to quantify how many fluorescent particles are on them. However, if the scale is too low it may cause the fluorescent particles on most surfaces to be undetectable, and if it is too high it may mean moderate and heavy contaminations are indistinguishable.

Third, unlike microorganisms, fluorescent particles do not naturally die on surfaces, which can lead to an overestimation of surface contaminations. The inactivation of noroviruses was relatively low during the 2.5-hour flight [51], so the overestimation was not serious. Nevertheless, it may not be proper to use fluorescent particles as surrogate indicators to model the spread of pathogens that are rapidly inactivated on surfaces, such as influenza viruses [52], or to model a long-period transmission, such as the 9-day SARS nosocomial outbreak [53].

Finally, our benchtop experiments cannot be used to study human touching behavior, which is assumed to be known in our experiments. More observational studies of human touching behavior are required.

4. Conclusions

In this study, a novel benchtop experiment was designed to explore the dynamic transmission of contaminants on multiple environmental surfaces due to touching. This experimental study provided mechanism-based evidence for the important role played by environmental surfaces in the transmission of contaminants, and confirmed the findings from multi-agent simulations. The diffusion of contaminated surfaces was found to follow an *S*-shaped logistic curve in time. In addition, aisle seats were found to be more contaminated than non-aisle seats with our assumed passenger touch behavior. These results could help to develop appropriate surface hygiene measures in indoor environments such as air cabins. Our benchtop experiments and associated approaches could be applied to studies of fomite transmission in other short-period outbreaks of pathogens with relatively high persistence on surfaces.

Acknowledgements

This project is supported by a RGC grant (No 17211615) of the Hong Kong SAR government.

References

[1] H. Guo, S. Lee, L. Chan, W. Li, Risk assessment of exposure to volatile organic compounds in different indoor environments, Environ. Res. 94 (2004) 57-66.

[2] S.F. Dowell, J.M. Simmerman, D.D. Erdman, J.-S.J. Wu, A. Chaovavanich, M. Javadi, J.-Y. Yang, L.J. Anderson, S. Tong, M.S. Ho, Severe acute respiratory syndrome coronavirus on hospital surfaces, Clin. Infect. Dis. 39 (2004) 652-657.

[3] S. Clay, S. Maherchandani, Y.S. Malik, S.M. Goyal, Survival on uncommon fomites of feline calicivirus, a surrogate of noroviruses, Am. J. Infect. Control 34 (2006) 41-43.

[4] S.-H. Kim, S.Y. Chang, M. Sung, J.H. Park, H.B. Kim, H. Lee, J.-P. Choi, W.S. Choi, J.-Y.

Min, Extensive viable Middle East respiratory syndrome (MERS) coronavirus contamination in air and surrounding environment in MERS isolation wards, Clin. Infect. Dis. 63 (2016) 363-369.

[5] T. Shiomori, H. Miyamoto, K. Makishima, M. Yoshida, T. Fujiyoshi, T. Udaka, T. Inaba, N. Hiraki, Evaluation of bedmaking-related airborne and surface methicillin-resistant Staphylococcus aureus contamination, J. Hosp. Infect. 50 (2002) 30-35.

[6] E. Scott, S. Duty, M. Callahan, A pilot study to isolate Staphylococcus aureus and methicillin-resistant S aureus from environmental surfaces in the home, Am. J. Infect. Control 36 (2008) 458-460.

[7] A.L. Pasanen, A review: fungal exposure assessment in indoor environments, Indoor air 11 (2001) 87-98.

[8] J.M. Portnoy, C.S. Barnes, K. Kennedy, Sampling for indoor fungi, J. Allergy. Clin. Immunol. 113 (2004) 189-198.

[9] A. Kramer, I. Schwebke, G. Kampf, How long do nosocomial pathogens persist on inanimate surfaces? A systematic review, BMC Infect. Dis. 6 (2006) 130.

[10] N. Van Doremalen, T. Bushmaker, V. Munster, Stability of Middle East respiratory syndrome coronavirus (MERS-CoV) under different environmental conditions, Eurosurveillance. 18 (2013) 20590.

[11] M. Nicas, R.M. Jones, Relative contributions of four exposure pathways to influenza infection risk, Risk Anal. 29 (2009) 1292-1303.

[12] F.S. Rhame, The inanimate environment, in: J.V. Bennett, P.S. Brachman (Eds.), Hospital Infections, fourth ed., Philadelphia: Lippincott-Raven, 1998, pp. 299-324.

[13] J.A. Otter, S. Yezli, G.L. French, The role played by contaminated surfaces in the transmission of nosocomial pathogens, Infect. Control Hosp. Epidemiol. 32 (2011) 687-699.

[14] J.A. Otter, S. Yezli, J.A. Salkeld, G.L. French, Evidence that contaminated surfaces contribute to the transmission of hospital pathogens and an overview of strategies to address contaminated surfaces in hospital settings, Am. J. Infect. Control 41 (2013) S6-S11.

[15] S.S. Huang, R. Datta, R. Platt, Risk of acquiring antibiotic-resistant bacteria from prior room occupants, Arch. Intern. Med. 166 (2006) 1945-1951.

[16] S. Nseir, C. Blazejewski, R. Lubret, F. Wallet, R. Courcol, A. Durocher, Risk of acquiring multidrug-resistant Gram-negative bacilli from prior room occupants in the intensive care unit, Clin. Microbiol. Infect. 17 (2011) 1201-1208.

[17] W. Seto, D. Tsang, R. Yung, T. Ching, T. Ng, M. Ho, L. Ho, J. Peiris, A.o.E.S.g.o.H. Authority, Effectiveness of precautions against droplets and contact in prevention of nosocomial transmission of severe acute respiratory syndrome (SARS), Lancet 361 (2003) 1519-1520.

[18] S.F. Bloomfield, A.E. Aiello, B. Cookson, C. O'boyle, E.L. Larson, The effectiveness of hand hygiene procedures in reducing the risks of infections in home and community settings including handwashing and alcohol-based hand sanitizers, Am. J. Infect. Control 35 (2007) S27-S64.

[19] M. Denton, M. Wilcox, P. Parnell, D. Green, V. Keer, P. Hawkey, I. Evans, P. Murphy, Role of environmental cleaning in controlling an outbreak of Acinetobacter baumannii on a neurosurgical intensive care unit, J. Hosp. Infect. 56 (2004) 106-110.

[20] H.L. Kirking, J. Cortes, S. Burrer, A.J. Hall, N.J. Cohen, H. Lipman, C. Kim, E.R. Daly, D.B. Fishbein, Likely transmission of norovirus on an airplane, October 2008, Clin. Infect.

Dis. 50 (2010) 1216-1221.
[21] S.A. Boone, C.P. Gerba, Significance of fomites in the spread of respiratory and enteric viral disease, Appl. Environ. Microbiol. 73 (2007) 1687-1696.
[22] H. Lei, Y. Li, S. Xiao, X. Yang, C.H. Lin, S.L. Norris, D. Wei, Z. Hu, S. Ji, Logistic growth of a surface contamination network and its role in disease spread, Sci. Rep. 7 (2017) 14826.
[23] M. Nicas, G. Sun, An integrated model of infection risk in a health-care environment, Risk Anal. 26 (2006) 1085-1096.
[24] M.P. Atkinson, L.M. Wein, Quantifying the routes of transmission for pandemic influenza, Bull. Math. Biol. 70 (2008) 820-867.
[25] S. Xiao, Y. Li, M. Sung, J. Wei, Z. Yang, A study of the probable transmission routes of MERS-CoV during the first hospital outbreak in the Republic of Korea, Indoor Air. doi: 10.1111/ina.12430.
[26] S. Okabe, H. Satoh, Y. Watanabe, In situ analysis of nitrifying biofilms as determined by in situ hybridization and the use of microelectrodes, Appl. Environ. Microbiol. 65 (1999) 3182-3191.
[27] T. Zhang, H.H. Fang, Applications of real-time polymerase chain reaction for quantification of microorganisms in environmental samples, Appl. Microbiol. Biotechnol. 70 (2006) 281-289.
[28] D.G. Oelberg, S.E. Joyner, X. Jiang, D. Laborde, M.P. Islam, L.K. Pickering, Detection of pathogen transmission in neonatal nurseries using DNA markers as surrogate indicators, Pediatr. 105 (2000) 311-315.
[29] W.A. Ivancic, M.G. Nishioka, R.H. Barnes, E.C. Hubal, M. Morara, S.M. Bortnick, Development and evaluation of a quantitative video-fluorescence imaging system and fluorescent tracer for measuring transfer of pesticide residues from surfaces to hands with repeated contacts, Ann. Occup. Hyg. 48 (2004) 519-532.
[30] E.A.C. Hubal, J.C. Suggs, M.G. Nishioka, W.A. Ivancic, Characterizing residue transfer efficiencies using a fluorescent imaging technique, J. Expo. Sci. Environ. Epidemiol. 15 (2005) 261-270.
[31] E. Andrews, A. Finney, R. Mosher, S. Samreth, Fluorescent marker and measurement system for quantitatively determining hand hygiene proficiency with use of alcohol-based hand sanitizer. http://bmedesign.engr.wisc.edu/projects/file/?fid=386/, 2008 (acessed 17.03.12).
[32] J. Wei, Y. Li, Enhanced spread of expiratory droplets by turbulence in a cough jet, Build. Environ. 93 (2015) 86-96.
[33] G.U. Lopez, Transfer of microorganisms from fomites to hands and risk assessment of contaminated and disinfected surfaces (Doctoral thesis), Tucson, Arizona: University of Arizona, 2013.
[34] G.U. Lopez, C.P. Gerba, A.H. Tamimi, M. Kitajima, S.L. Maxwell, J.B. Rose, Transfer efficiency of bacteria and viruses from porous and nonporous fomites to fingers under different relative humidity conditions, Appl. Environ. Microbiol. 79 (2013) 5728-5734.
[35] M. Covington, Curve Shape in Digital Photography. http://www.covingtoninnovations.com/dslr/Curves.html, 2004 (accessed 17.12.01).
[36] Q. Cao, Y. Liu, W. Liu, C.H. Lin, D. Wei, S. Baughcum, S. Norris, X. Shen, Z. Long, Q. Chen, Experimental study of particle deposition in the environmental control systems of commercial airliners, Build. Environ. 96 (2016) 62-71.

[37] F.J. Massey Jr, The Kolmogorov-Smirnov test for goodness of fit, J. Am. Stat. Assoc. 46 (1951) 68-78.
[38] X. Zhang, Finger movements based on biometric authentication for touch devices (Master thesis), Oslo, Norway: University of Oslo, 2011.
[39] C. Mackintosh, P. Hoffman, An extended model for transfer of micro-organisms via the hands: differences between organisms and the effect of alcohol disinfection, J. Hyg. 92 (1984) 345-355.
[40] T. Julian, J. Leckie, A. Boehm, Virus transfer between fingerpads and fomites, J. Appl. Microbiol. 109 (2010) 1868-1874.
[41] P. Rusin, S. Maxwell, C. Gerba, Comparative surface-to-hand and fingertip-to-mouth transfer efficiency of gram-positive bacteria, gram-negative bacteria, and phage, J. Appl. Microbiol. 93 (2002) 585-592.
[42] J.N. Mbithi, V.S. Springthorpe, J.R. Boulet, S.A. Sattar, Survival of hepatitis A virus on human hands and its transfer on contact with animate and inanimate surfaces, J. Clin. Microbiol. 30 (1992) 757-763.
[43] J.F. Kenney, E.S. Keeping, Mathematics of statistics, second ed., Van Nostrand, New York, 1951.
[44] D.R. Legates, G.J. McCabe, Evaluating the use of "goodness-of-fit" measures in hydrologic and hydroclimatic model validation, Water Resour. Res. 35 (1999) 233-241.
[45] S.J. Dancer, The role of environmental cleaning in the control of hospital-acquired infection, J. Hosp. Infect. 73 (2009) 378-385.
[46] A.N. Duckro, D.W. Blom, E.A. Lyle, R.A. Weinstein, M.K. Hayden, Transfer of vancomycin-resistant enterococci via health care worker hands, Arch. Intern. Med. 165 (2005) 302-307.
[47] C. Adams, J. Smith, V. Watson, C. Robertson, S. Dancer, Examining the association between surface bioburden and frequently touched sites in intensive care, J. Hosp. Infect. 95 (2017) 76-80.
[48] L. Sehulster, R.Y. Chinn, M. Arduino, J. Carpenter, R. Donlan, D. Ashford, R. Besser, B. Fields, M. McNeil, C. Whitney, Guidelines for environmental infection control in health-care facilities, MMWR. Recomm. Rep. 55 (2003) 1-42.
[49] E. Riley, G. Murphy, R. Riley, Airborne spread of measles in a suburban elementary school, Am. J. Epidemiol. 107 (1978) 421-432.
[50] H. Qian, Y. Li, P.V. Nielsen, X. Huang, Spatial distribution of infection risk of SARS transmission in a hospital ward, Build. Environ. 44 (2009) 1651-1658.
[51] P. Liu, Y.-W. Chien, E. Papafragkou, H.-M. Hsiao, L.-A. Jaykus, C. Moe, Persistence of human noroviruses on food preparation surfaces and human hands, Food Environ. Virol. 1 (2009) 141-147.
[52] B. Bean, B. Moore, B. Sterner, L. Peterson, D. Gerding, H. Balfour, Survival of influenza viruses on environmental surfaces, J. Infect. Dis. 146 (1982) 47-51.
[53] S. Xiao, Y. Li, T.W. Wong, D.S.C. Hui. Role of fomites in SARS transmission during the largest hospital outbreak in Hong Kong, PLoS One 12 (2017) e0181558.

Supplementary information

Characterizing dynamic transmission of contaminants on a surface touch network

Shenglan Xiao[a,*], Yuguo Li[a], Hao Lei[a], ChaoHsin Lin[b], Sharon L Norris[b], Xinyan Yang[a], Pengcheng Zhao[a]

[a] Department of Mechanical Engineering, The University of Hong Kong, Pokfulam Road, Hong Kong SAR, China
[b] Environmental Control Systems, Boeing Commercial Airplanes, Everett, WA, USA

* Corresponding author:
Shenglan Xiao. E-mail: u3002980@hku.hk; Tel.: +852 60992752

SI A. Supplemental tables

Table S1 Parameter values for the passenger behavior in the experiments.

Parameters	Descriptions	Values [a]
P_{tasb}	Probability that an individual touches certain aisle seatback surfaces on the way to toilets and back	1/6
f_{st}	Frequency for susceptible individuals to use toilets (1/hr) [b]	1/6
$f_h^{i,sb}$	Frequency for individual i to touch the immediate front seatback surfaces (1/hr) [c]	3
$f_h^{i,as}$	Frequency for individual i to touch the armrest surfaces (1/hr) [d]	5
$f_h^{i,tt}$	Frequency for individual i to touch the tray table surfaces (1/hr) [e]	4

a The source of parameter values is Lei et al. [1];

b During the cruise period of 2.5 hours, there were assumed to be 50 susceptible individuals going to toilets. According to Kirking et al. [2], all six infectors in this outbreak had used toilets. Therefore 56 passengers in total used the toilets;

c During the cruise period of 2.5 hours, every passenger was assumed to touch the immediate front seatback surfaces 8 (≈3×2.5) times;

d During the cruise period of 2.5 hours, every passenger was assumed to touch the armrest surfaces 13 (≈5×2.5) times;

e During the cruise period of 2.5 hours, every passenger was assumed to touch the tray table surfaces 10 (=4×2.5) times.

Table S2 The sequences for passengers to touch aisle seatback surfaces on the way to toilets and back in Fig. S6.

Rounds [a]	**Passengers** [b]	**Sequences to touch surfaces** [c]
1	P-8B	S-7B → S-7C → S-8C → S-11D → S-14D → S-15D → S-16D → S-17D → S-20C → S-21C → S-22D → S-24D → TS-2 → S-24C → S-22C → S-19D → S-18C → S-16C → S-14C → S-12C → S-10D → S-9D → S-7C → S-7B
2	P-11D	S-10D → S-12D → S-13D → S-14D → S-16C → S-18C → S-19C → S-21D → S-24D → S-26C → TS-1 → S-24D → S-22C → S-21C → S-20C → S-19C → S-17D → S-14D → S-13C → S-10D
3	P-25C	S-24C → TS-2 → S-25D → S-24C
4	P-17E	S-16E → S-16D → S-18D → S-20D → S-21D → S-24D → TS-2 → S-24D → S-22C → S-20D → S-17D → S-16D → S-16E
5	P-15A	S-14A → S-14B → S-14C → S-17D → S-19D → S-22D → S-25D → TS-1 → S-26C → S-25C → S-23D → S-21D → S-20C → S-18D → S-17D → S-15D → S-14C → S-14B → S-14A
6	P-12F	S-11F → S-11E → S-11D → S-13D → S-16D → S-17D → S-18C → S-20D → S-23D → S-24D → S-26C → TS-1 → S-26D → S-23D → S-22D → S-19D → S-18C → S-17C → S-16C → S-15D → S-13D → S-11D → S-11E → S-11F
7	P-19E	S-18E → S-18D → S-21D → S-22D → S-23D → S-26D → TS-1 → S-24C → S-23D → S-22C → S-21C → S-18D → S-18E
8	P-9E	S-8E → S-8D → S-11D → S-12C → S-13C → S-16D → S-18D → S-20C → S-23C → S-26C → TS-2 → S-25D → S-22C → S-20D → S-17D → S-16D → S-15D → S-12D → S-9C → S-8D → S-8E
9	P-19D	S-18D → S-19D → S-22D → S-24D → S-26D → TS-2 → S-24D → S-21D → S-19C → S-18D
10	P-16C	S-15C → S-16C → S-18C → S-20D → S-23C → S-24C → TS-1 → S-25C → S-22D → S-21C → S-19D → S-16D → S-15C
11	P-18F	S-17F → S-17E → S-17D → S-18D → S-21C → S-23C → S-25D → TS-2 → S-24C → S-23C → S-20C → S-18D → S-17D → S-17E → S-17F

12	P-26F	S-25F → S-25E → S-25D → TS-1 → S-25D → S-25E → S-25F
13	P-23B	S-22B → S-22C → S-25D → S-26D → TS-1 → S-26D → S-25D → S-23D → S-22C → S-22B
14	P-17F	S-16F → S-16E → S-16D → S-17D → S-18C → S-19C → S-22C → S-23D → S-25D → TS-2 → S-25D → S-23D → S-22D → S-19D → S-16D → S-16E → S-16F
15	P-23F	S-22F → S-22E → S-22D → S-23D → S-25D → TS-2 → S-24D → S-23D → S-22D → S-22E → S-22F
16	P-21F	S-20F → S-20E → S-20D → S-23D → S-25C → TS-2 → S-26C → S-24C → S-21C → S-20D → S-20E → S-20F
17	P-20E	S-19C → S-21D → S-24D → S-25C → TS-1 → S-24D → S-22C → S-21D → S-19C
18	P-16F	S-15F → S-15E → S-15D → S-17C → S-19D → S-20D → S-23D → S-26C → TS-2 → S-26D → S-24C → S-21C → S-19C → S-16D → S-15D → S-15E → S-15F
19	P-15D	S-14D → S-16C → S-19C → S-22D → S-23D → S-25C → TS-2 → S-24C → S-22D → S-21D → S-18D → S-17D → S-14D
20	P-23E	S-22E → S-22D → S-24C → S-26C → TS-2 → S-24C → S-22D → S-22E
21	P-12C	S-11C → S-14D → S-16D → S-17D → S-20C → S-21D → S-24D → TS-1 → S-26C → S-24C → S-22D → S-19D → S-18C → S-17D → S-14D → S-12C →S-11C
22	P-23C	S-22C → S-24C → S-25D → TS-2 → S-26D → S-24D → S-23D → S-22C
23	P-16A	S-15A → S-15B → S-15C → S-18D → S-19D → S-20D → S-23D → S-24C → S-25C → S-26D → TS-1 → S-26D → S-25D → S-24C → S-23C → S-20D → S-18C → S-17C → S-15C → S-15B → S-15A
24	P-18E	S-17E → S-17D → S-20D → S-23D → S-24D → S-25C → TS-2 → S-26C → S-23D → S-21C → S-20C → S-17D → S-17E
25	P-7D	S-6D → S-9D → S-12C → S-13D → S-16D → S-17C → S-20C → S-22C → S-23D → S-25D → TS-1 → S-25D → S-23C → S-22C → S-20C → S-17D → S-15D → S-12C →

		S-9D → S-8C → S-6D
26	P-24B	S-23B → S-23C → S-24C → TS-2 → S-26C → S-24C → S-23C → S-23B
27	P-17B	S-16B → S-16C → S-17D → S-19C → S-21D → S-24D → S-25D→ S-26D → TS-1 → S-24C → S-21D → S-19C → S-17D → S-16C → S-16B
28	P-15E	S-14E → S-14D → S-15C → S-17C → S-18D → S-19D → S-22D→ S-25C → TS-2 → S-25C → S-23D → S-22C → S-21C → S-20D → S-17C → S-14D → S-14E
29	P-20F	S-19F → S-19E → S-19D → S-20D → S-22C → S-25C → S-26C→ TS-1 → S-24D → S-23D → S-22C → S-19D → S-19E → S-19F
30	P-13E	S-12E → S-12D → S-13C → S-16D → S-17D → S-18D → S-19D → S-21C → S-22D → S-24C → S-26C → TS-2 → S-24C → S-22C → S-20C → S-17D → S-15C → S-13C → S-12D → S-12E
31	P-13B	S-12B → S-12C → S-15D → S-16D → S-17D → S-19D → S-22D → S-23D → S-26D → TS-1 → S-24C → S-23D → S-21C → S-20C → S-17C → S-14C → S-12C → S-12B
32	P-9C	S-8C → S-9D → S-10C → S-12D → S-15C → S-16D → S-18D → S-21D → S-22C → S-25C → TS-1 → S-25D → S-23D → S-21D → S-18D → S-16C → S-14D → S-13D → S-12D → S-11C → S-10C → S-8C
33	P-10E	S-9E → S-9D → S-12C → S-13C → S-15D → S-16C → S-18C → S-20D → S-23C → S-25D → TS-2 → S-24D → S-23D → S-20D → S-18D → S-16C → S-13D → S-11C → S-10C → S-9D → S-9E
34	P-19A	S-18A → S-18B → S-18C → S-21C → S-24C → TS-2 → S-25C → S-22D → S-19D → S-18C → S-18B → S-18A
35	P-11F	S-10F → S-10E → S-10D → S-11C → S-13D → S-14C → S-15C → S-17D → S-19C → S-21D → S-22D → S-25D → TS-1 → S-24C → S-23D → S-22C → S-19C → S-18C → S-17D → S-16C → S-13C → S-12D → S-11D → S-10D → S-10E → S-10F
36	P-24C	S-23C → S-25C → TS-1 → S-25C → S-23C
37	P-24D	S-23D → S-25D → TS-1 → S-24D → S-23D

38	P-15C	S-14C → S-15D → S-16D → S-18C → S-21D → S-22D → S-24C→ S-25D → TS-2 → S-25C → S-23D → S-21D → S-19D → S-18C → S-15D → S-14C
39	P-19C	S-18C → S-20D → S-21D → S-24C → TS-1 → S-25C → S-24C → S-22C → S-20C → S-18C
40	P-6A	S-6C → S-9D → S-11C → S-12D → S-14C → S-17D → S-20C → S-23D → S-24D → TS-2 → S-25C → S-23D → S-21D → S-20D → S-19D → S-17C → S-16C → S-15D → S-13D → S-11D → S-9C → S-6C
41	P-7E	S-6E → S-6D → S-9D → S-11C → S-12C → S-14C → S-15D → S-17C → S-20C → S-22C → S-23C → S-25C → TS-2 → S-26D → S-25D → S-23D → S-21C → S-20D → S-19D → S-16D → S-15D → S-12C → S-11C → S-9C → S-8D → S-7D → S-6D → S-6E
42	P-17A	S-16A → S-16B → S-16C → S-19C → S-21D → S-24C → S-25C→ S-26D → TS-2 → S-25C → S-23D → S-21D → S-19C → S-16C → S-16B → S-16A
43	P-6D	S-7C → S-9C → S-10D → S-13D → S-16D → S-19D → S-22C → S-24D → TS-2 → S-24D → S-21D → S-20C → S-18D → S-17D → S-15D → S-14C → S-12C → S-11D → S-9D → S-8D → S-6C
44	P-8E	S-7E → S-7D → S-8C → S-11C → S-13D → S-14C → S-15C → S-17D → S-20C → S-21C → S-24D → S-25D → S-26D → TS-1 → S-25D → S-22C → S-19C → S-18C → S-16C → S-13D → S-11D → S-9D → S-8C → S-7D → S-7E
45	P-17C	S-16C → S-18C → S-20D → S-21C → S-24D → S-25D → S-26C→ TS-2 → S-24C → S-21D → S-20C → S-18C → S-16C
46	P-16E	S-15E → S-15D → S-17C → S-18D → S-20C → S-21D → S-22D → S-23C → S-26C → TS-2 → S-24D → S-23D → S-21D → S-19C → S-18D → S-17D → S-16C → S-15D → S-15E
47	P-7C	S-6C → S-9D → S-12C → S-14C → S-16C → S-17D → S-18C → S-20D → S-21C → S-23D → S-25D → TS-2 → S-25C → S-24D → S-22C → S-21C → S-19D → S-16D → S-14C → S-12D → S-9D → S-8C → S-6C
48	P-22F	S-21F → S-21E → S-21D → S-24D → TS-2 → S-25D →

		S-24D → S-21D → S-21E → S-21F
49	P-25D	S-24D → S-25D → S-26C → TS-2 → S-25C → S-24D
50	P-20D	S-19D → S-20D → S-22C → S-24C → S-26C → TS-2 → S-25D → S-22D → S-21D → S-19D
51	P-26E	S-25E → S-25D → TS-2 → S-25D → S-25E
52	P-6F	S-8D → S-10D → S-12C → S-14C → S-17D → S-20C → S-22C → S-24C → TS-2 → S-24C → S-22D → S-21C → S-19C → S-18D → S-15C → S-14C → S-12C → S-11D → S-9C → S-8D → S-6D
53	P-18C	S-17C → S-19C → S-22C → S-24C → TS-2 → S-26D → S-24C → S-21C → S-20C → S-19C → S-18D → S-17C
54	P-6C	S-6C → S-8C → S-9D → S-11C → S-13D → S-15C → S-16C → S-18C → S-21D → S-23C → S-24D → S-26C → TS-1 → S-25D → S-22D → S-19D → S-16D → S-13C → S-12C → S-9D → S-7D
55	P-22C	S-21C → S-24D → TS-1 → S-25D → S-24D → S-21C
56	P-17D	S-16D → S-19C → S-20D → S-21C → S-24C → S-25C → TS-2 → S-26D → S-24C → S-22D → S-19D → S-18D → S-16D

a We assumed 56 passengers spent the same time using toilets, so we divided the flight cruise period into 56 rounds. One round represents about 2.68 minutes;

b P-XY represents the passenger seating in Row Y and Column X. The arrangement of seats in economy class can be seen in Fig. 3B;

c S-XY represents the seatback surfaces of seats in Row Y and Column X. TS-X represents the Xth toilets. The arrangement of seats and toilets in economy class can be seen in Fig. 3B.

Table S3 Parameter values for the simulation of fluorescent particles transmission in the benchtop experiments.

Parameter	**Description**	**Value**
L_0	Initial amounts of fluorescent particles on index patients' fingerstalls (g)	0.6
b_h	First-order inactivation rate on hands (1/hr)	0 [a]
b_p	First-order inactivation rate on porous surfaces (1/hr)	0 [a]
b_{np}	First-order inactivation rate on non-porous surfaces (1/hr)	0 [a]

b_w	First-order inactivation rate on wet surfaces (1/hr)	0 [a]
f	Finger touching forces (N)	$f \sim N(11.80, 1.97^2)$ [b]
A_f	Contact area of a fingerstall (cm^2)	2.0
A_{sb}	Surface area of a seatback (cm^2)	19.3
A_{as}	Surface area of an armrest (cm^2)	9.0
A_{tt}	Surface area of a tray table (cm^2)	37.4
A_{ts}	Surface area of a toilet (cm^2)	673.2

a Unlike microorganisms, fluorescent particles do not naturally die on surfaces.

b The source is Fig. S3.

SI B. Supplemental figures

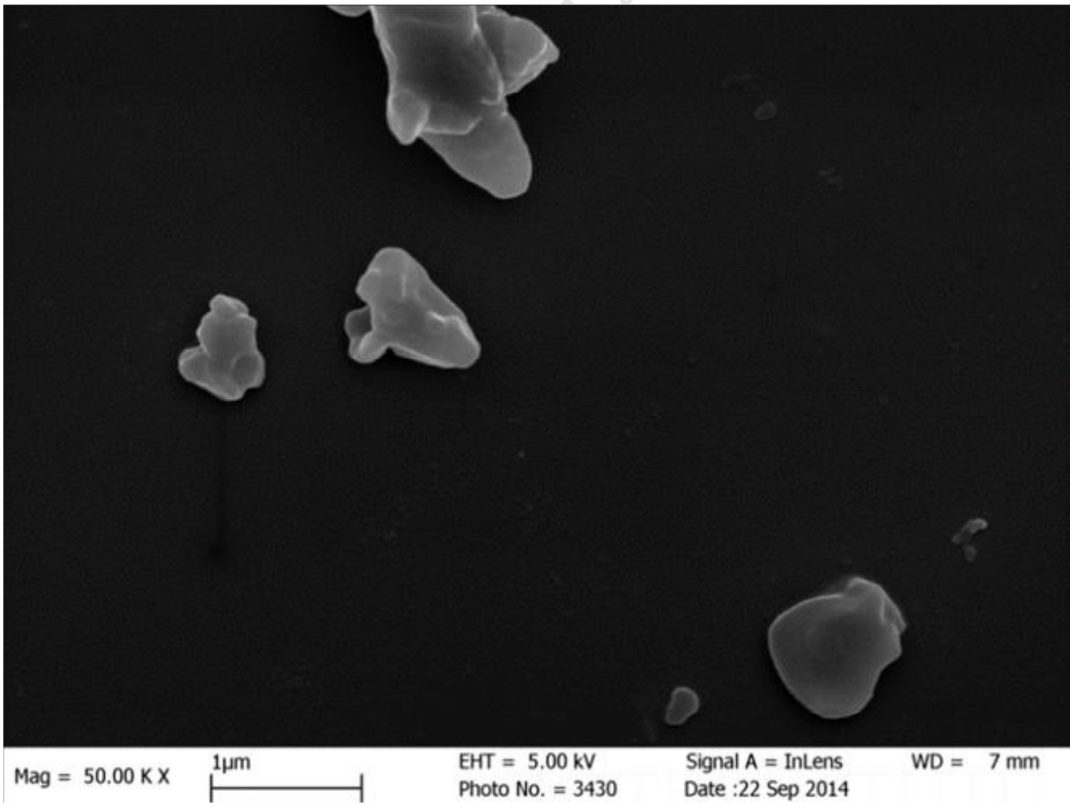

Fig. S1. The magnified image of fluorescent particles from GloGerm™ taken by scanning

electron microscopy (SEM).

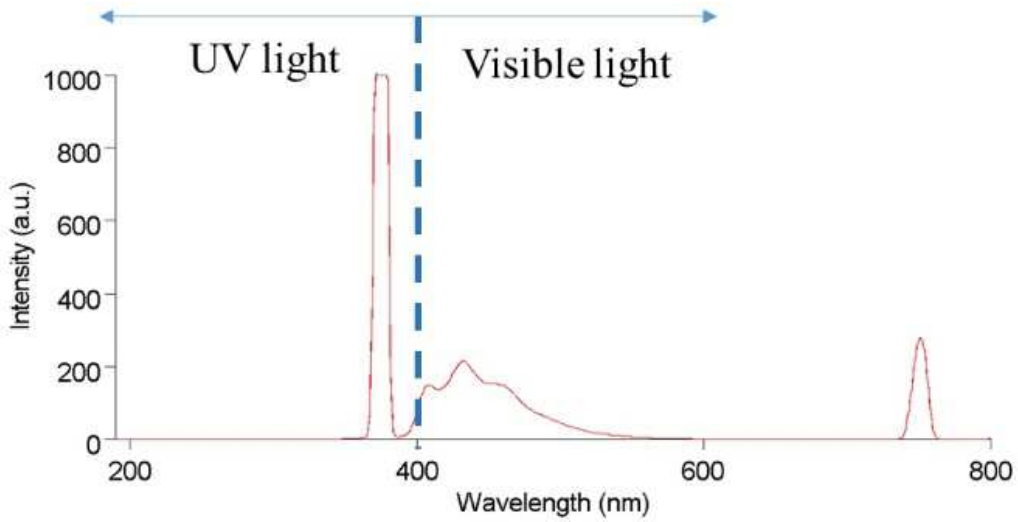

(A)

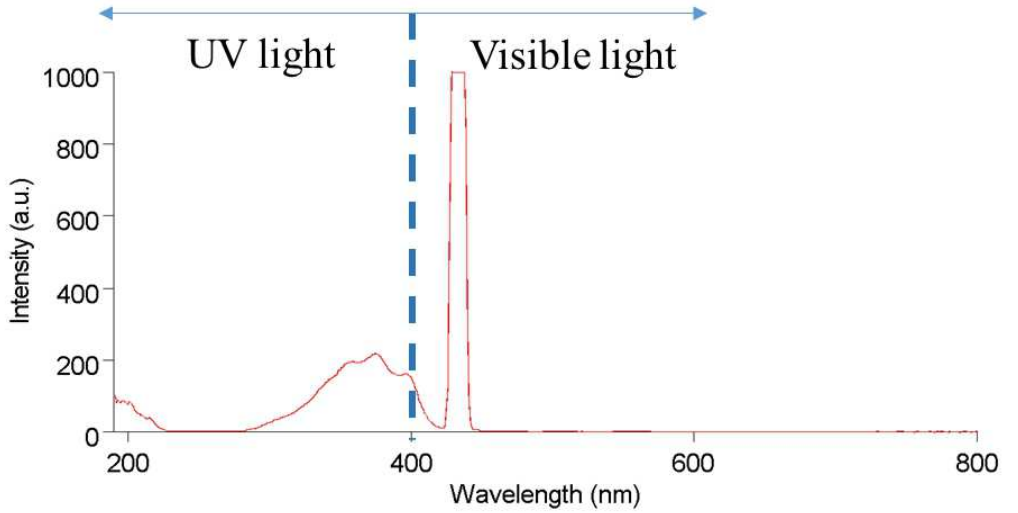

(B)

Fig. S2. (A) The relationship between excitation light wavelength and emitted light intensity; (B) the relationship between emitted light wavelength and emitted light intensity.

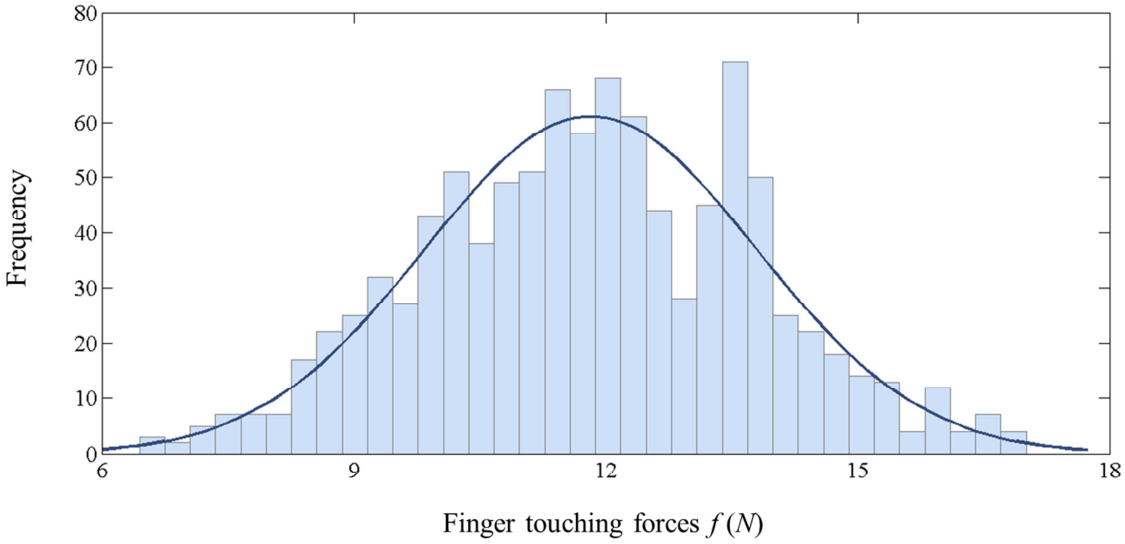

Fig. S3. The frequency distribution of finger touching forces for 1000 measurements. The histogram was fitted with a normal distribution, $N(11.80, 1.97^2)$.

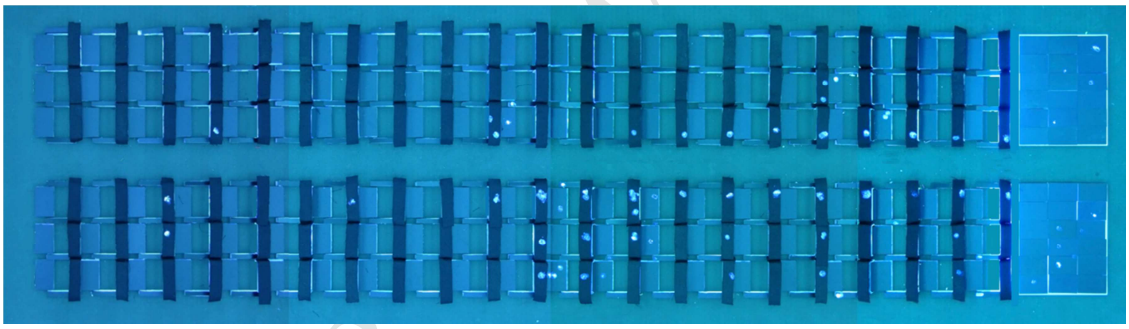

(A)

(B)

Fig. S4. (A) The combination of four original photos by the four cameras. (B) The processed photo of fluorescent particles without the background.

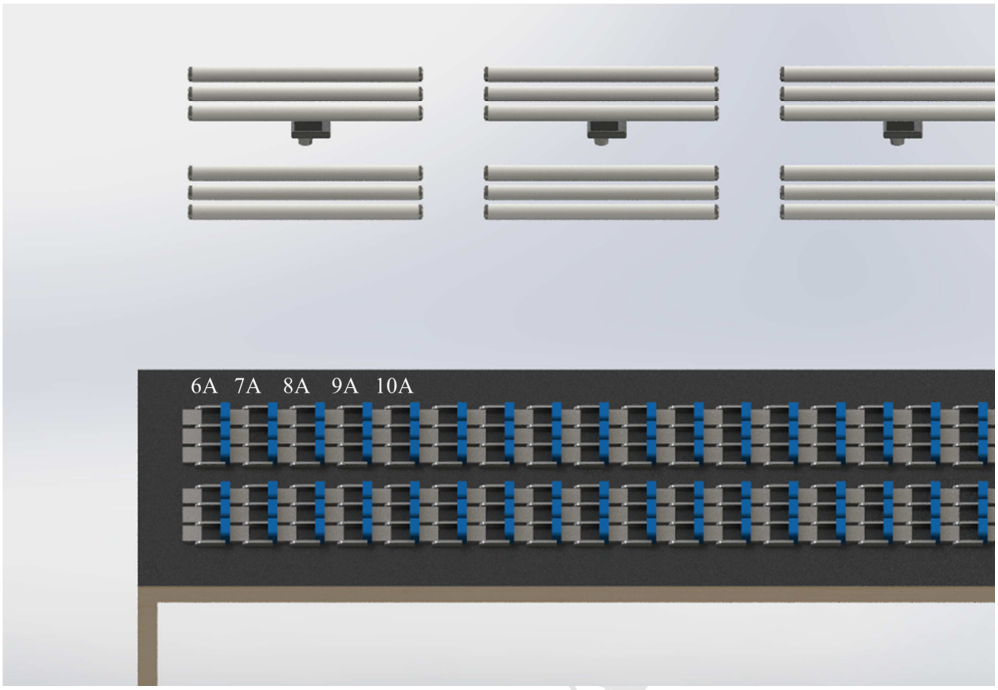

Fig. S5. Positions of Seats 6A, 7A, 8A, 9A and 10A, UV lamps and cameras.

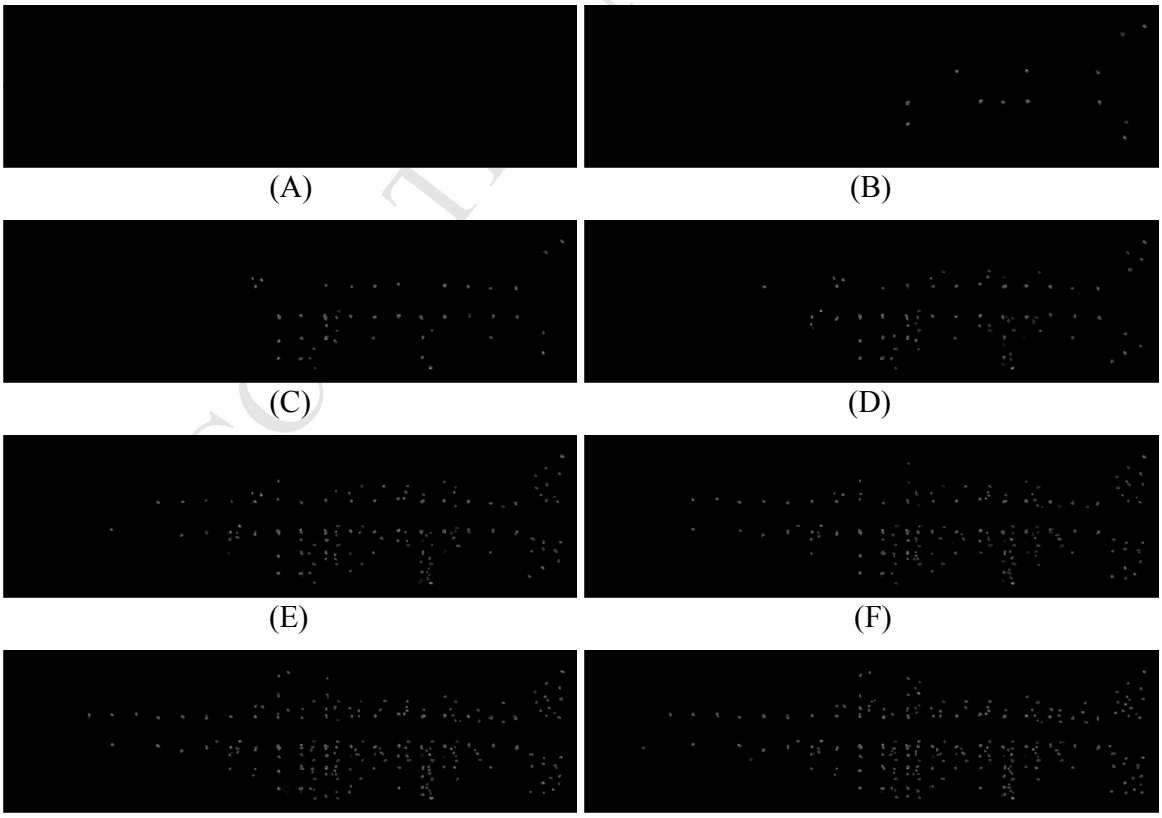

(G) (H)

Fig. S6. Processed photos showing fluorescent particles on surfaces in one experiment at different time points. (A) Round 0; (B) Round 8; (C) Round 16; (D) Round 24; (E) Round 32; (F) Round 40; (G) Round 48; (H) Round 56.

References for supplementary information

[1] H. Lei, Y. Li, S. Xiao, X. Yang, C.H. Lin, S.L. Norris, D. Wei, Z. Hu, S. Ji, Logistic growth of a surface contamination network and its role in disease spread, Sci. Rep. 7 (2017) 14826.

[2] H.L. Kirking, J. Cortes, S. Burrer, A.J. Hall, N.J. Cohen, H. Lipman, C. Kim, E.R. Daly, D.B. Fishbein, Likely transmission of norovirus on an airplane, October 2008, Clin. Infect. Dis. 50(9) (2010) 1216-1221.

Characterizing dynamic transmission of contaminants on a surface touch network

Highlights

- A novel benchtop experiment was designed to study surface contamination
- The temporal diffusion of contaminated surfaces presents an *S*-shaped logistic curve
- Aisle seats are found to be more contaminated than non-aisle seats in air cabins
- Revealed a possible mechanism for fomite route of disease transmission